energies

MDPI

Article

Uplift Bearing Capacity of Cone-Cylinder Foundation for Transmission Line in Frozen Soil Regions, Using Reduced-Scale Model Tests and Numerical Simulations

Yangchun Han [1], Jiulong Cheng [1,*], Qiang Cui [2], Qianyun Dong [1] and Wanting Song [3]

[1] College of Geoscience and Surveying Engineering, China University of Mining and Technology (Beijing), Beijing 100083, China; hanycn@foxmail.com (Y.H.); dongqyun@foxmail.com (Q.D.)
[2] Power Transmission and Transformation Engineering Department, China Electric Power Research Institute, Beijing 102401, China; everjsl@126.com
[3] College of Humanity and Law, China University of Mining and Technology (Beijing), Beijing 100083, China; songwant@foxmail.com
* Correspondence: JLCheng@cumtb.edu.cn; Tel.: +86-010-6233-9216

Received: 13 February 2020; Accepted: 16 April 2020; Published: 21 April 2020

Abstract: In order to analyze the uplift bearing capacity of cone-cylinder foundation for transmission line in frozen soil regions, a series of reduced-scale modeling tests and numerical simulations are carried out. First, three reduced-scale cone-cylinder foundations with the same sizes, that are five times smaller than the prototype, are made and then loaded under uplift load at −5 °C, −10 °C, and −15 °C, respectively. On this basis, the foundations of nine sizes are modeled and loaded by numerical simulation. The impact of three dimension factors, including the ratio of depth to bottom width ($\lambda = h_t/D_t$), the top diameter of the cone-cylinder (d), and the bottom diameter of the cone-cylinder (D), on the uplift bearing capacity of foundations have been investigated. The results reveal that, for cone-cylinder foundation, the uplift bearing capacity is obviously affected by the freezing temperatures and the foundation sizes. The capacity is negatively correlated with the former. Whereas the order of correlation with the latter is as follows: λ, D, and d based on the comprehensive results of range and variance analysis, but none of them are the significant factors, according to the F-test. Furthermore, three failure mechanisms of frozen soil are distinguished and named T-mode, V-mode, and U-mode, respectively. Based on the above results, the bearing mechanism of cone-cylinder foundation in frozen soil is elaborated in detail.

Keywords: power transmission line; ultimate uplift load; frozen soil; reduced-scale modeling test; numerical modeling

1. Introduction

The construction of transmission lines in the Tibetan Plateau has been going on for decades in China, and it is still advancing today. The foundations of are usually embedded in the permafrost, which is a special kind of soil that is very sensitive to temperature, rainfall, human disturbance and so on [1,2]. The frost heave and settlement caused by the repeated freeze-thaw action will significantly affect the stability of the foundation [3]. In view of the above situations, the cone-cylinder foundation (Figure 1b) with an oblique surface can significantly reduce the above effects [4]. Therefore, this foundation is widely used for the power transmission project from Qinghai to Tibet. The performance of its practical application, including the estimation of settlement [5], the freeze–thaw properties and thermal stability [6], the impact on the permafrost [7], and the displacement characteristics and mechanisms [8],

has been widely studied. Wen et al. [9] analyzed the influence of frost heaving force on the stress and deformation characteristics of tower foundations in Qinhai Tibet Plateau, and proposed that the use of thermosyphons may effectively reduce the settlement of the foundation, but will increase the risk of frost jacking.

(**a**) (**b**)

Figure 1. Construction of cone-cylinder foundation in Qinhai, China: (**a**) pouring concrete; (**b**) after concrete curing.

Moreover, dozens of experimental, numerical simulated, and theoretical works have been done, and the results indicate that the bearing performance is affected by many factors, for example: the material parameters of frozen soil and pile [10,11], the frost-heave effect [12,13], and the mechanical behavior of frozen soil-concrete interfaces [14,15]. Typically, Fei et al. [16] proposed a modified von-mises model to simulate the mechanical behavior of frozen silts, and the results reveal that the variation of the strain rate within the seasonally frozen soil had a significant impact on the performance of laterally loaded piles. Yang et al. [17] proposed an effective depth to fixity models, with several key parameters. However, the research on the uplift bearing capacity of the foundations in frozen soil, which is the controlling design factor for the transmission line towers [18], are quite insufficient. In addition, there are almost no investigations of the influence of geometric sizes on the bearing capacity of a foundation in permafrost.

In this study, the uplift bearing capacity of cone-cylinder foundations with nine different sizes is studied using numerical simulations, which are based on the data from reduced-scale modeling tests. Firstly, in Section 2, three reduced-scale foundations are assembled and then tested under axial uplift load at three freezing temperatures (−5 °C, −10 °C, and −15 °C). Secondly, in Section 3, based on the model test data, the numerical simulation of the foundations of nine sizes are carried out. Those foundations are designed using the principle of orthogonality. Three geometric dimension factors, including the ratio of depth to bottom width ($\lambda = h_t/D_t$), the top diameter of the cone-cylinder (d), and the bottom diameter of the cone-cylinder (D), are considered; and these factors are set at three levels. The uplift performance of these nine foundations is simulated and then analyzed from two aspects: the ultimate uplift load and the failure mechanisms of frozen soil. Based on the results of Sections 2 and 3, a comprehensive analysis on the bearing mechanism of cone-cylinder foundation in frozen soil is illustrated in Section 4. Finally, the conclusions of this paper are elaborated in Section 5, which can provide theoretical and data support for the design of cone-cylinder foundations for transmission towers in frozen soil regions.

2. Reduced-Scale Modeling Test

Under the natural conditions, the construction cycle of the test foundation often lasts nearly one year, including the process of excavation, pouring, maintenance, backfilling, and refreezing and so on [1,5]. Therefore, the reduced-scale modeling test is selected in this work, which is refer to in [19,20].

2.1. Pier Design and Soil Properties

As shown in Figure 2, a reduced-scale cone-cylinder foundation is designed to refer to the prototype (Figure 1), which is the general shape that has been widely used. The bottom width of former is about 1/5 of the latter, whereas the cone-cylinder in the model is designed for a larger diameter for further study. For example, improving the endothermic capacity of the foundation by filling the cone-cylinder with special materials. The model is made of stainless steel to ensure sufficient strength. The structure can be divided into three parts: the circular truncated cone, the connecting square tube, and the pressure-bearing square tube, and then connected with 21 shock-proof bolts. The inclination angle of the oblique surface is 7° to resist the influence of tangential frost-heave forces. A 12 mm diameter round hole is designed in the center of the top plate for bolting with the loading bar. A total of three models were fabricated to avoid the effect of the possible deformation of the reused foundation.

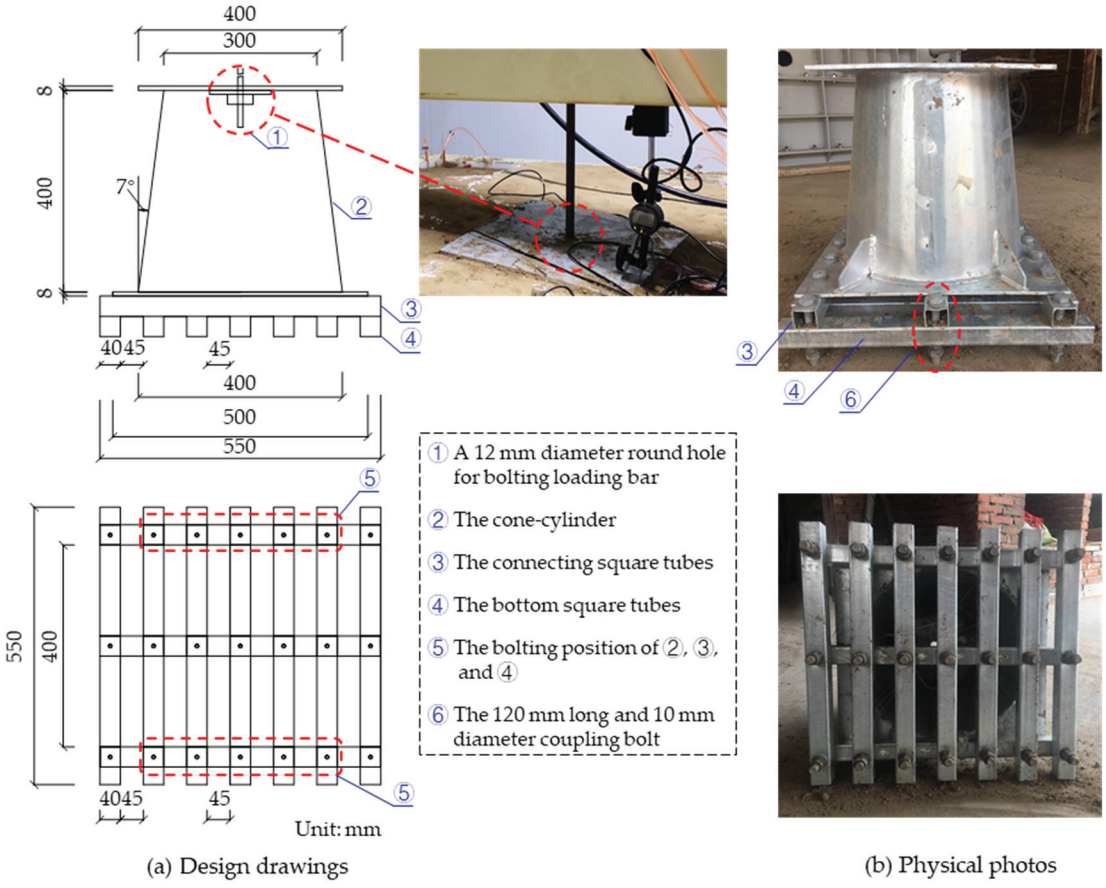

Figure 2. Design drawings and physical drawings of test foundation.

This study is based on the project of the power transmission line from Haibei to Yakeshi, that is located in Hulun Buir, Inner Mongolia, China. Hence, the soil samples are taken from a typical construction site along this line. A total of six tons of samples are collected; most of them are taken within −1 m underground, whereas a few are taken from −2 m and −3 m for a parameter test. The physical, mechanical, and thermodynamic properties of test soil samples are determined in the laboratory according to the specifications and standards of [21–26]. The results are listed in Tables 1–3.

According to the particle analysis test, it was determined that the composition, category, and particle grading of soil samples from three depths are relatively consistent, so the indoor model test adopts the soil within–1 m underground. The test results are also mainly for the soil at this depth, except for the direct shear tests (Table 2), which are carried out on three samples from −1 m, −2 m, and −3 m. The vertical pressure of the test is 50 kPa, 100 kPa, 150 kPa, 200 kPa, 300 kPa, and 400 kPa, respectively, and the shear rate is 1 mm/min. In short, the sample is silt with strong frost heaving and low salinity. Hence, the salt heaving will not occur.

Table 1. The physical, mechanical, and thermodynamic properties of test soil.

Category	No.	Test Items	Number of Tests	Test Results
Physical parameters tests	1	Particle size analysis	5	Fine-grained silt and well graded
	2	Nature density (g/cm^3)	3	1.42, 1.58, 1.49
	3	Moisture content (%)	5	5.5, 14.7, 5.8, 19.4, 6.53
	4	Specific gravity of soil particle	3	2.55, 2.54, 2.61
	5	Salt content test	2	Low salinity and no salt heaving
	6	Compressibility coefficient (Mpa^{-1})	1	0.17, medium compressibility
Mechanical parameters tests	7	Direct shear tests	3	As shown in Table 2
	8	Unconsolidated-undrained triaxial compression tests	3	As shown in Table 3
Thermodynamic parameters tests	9	Frost heave rate (%)	3	6, strong frost heaving
	10	Thermal conductivity (W/(m·K))	3	1.07
	11	Freezing temperature (°C)	2	−0.097

Table 2. Test results of direct shear.

Sampling Location	c (kPa)	φ (°)
Underground 1 m	3.78	10.70
Underground 2 m	5.88	10.37
Underground 3 m	9.86	11.97

Table 3. Test results of unconsolidated-undrained triaxial compression.

Compactness-Moisture Content	50/100/150 kPa		100/200/300 kPa	
	c (kPa)	φ (°)	c (kPa)	φ (°)
80–8%	22.8	33.4	30.2	30.5
85–8%	38.1	30.3	30.4	32.1
80–11%	28.0	30.6	19.3	29.6
85–11%	10.1	33.3	17.5	30.4
80–14%	13.2	23.9	9.4	26.1
85–14%	17.6	28.1	8.8	28.9
Mean value	21.6	29.9	19.2	29.6

2.2. Test Devices and Monitoring Apparatuses

2.2.1. Test Box and Loading System

Figure 3a shows the photo of the test box which is specially designed for the freezing-loading test. The length, width and height of the box are 2 m, 2 m and 1 m respectively. Figure 3b depicts the drawing of the loading system which can carry out uplift, lateral, and uplift-lateral composite loading. The loading frame composed of three beams, which can provide the reaction force of 300 kN, is installed in the middle of the box and bolted together. The vertical and fixed beam are both riveted to the integral frame, whereas the sliding beam can slide up and down along the groove on the vertical beam. In addition, three hydraulic jacks of 20 T are selected as the power source. In the process of uplift loading, two hydraulic jacks of 20 T are placed on the fixed beam symmetrically. The uplift load

can be transferred to the loading bar through the sliding beam and then applied to the test foundation. In the process of lateral loading, the horizontal force is transmitted by the cushion block. When the two systems described above work at the same time, the uplift-lateral composite load can be applied. Only uplift loading function is used in this work.

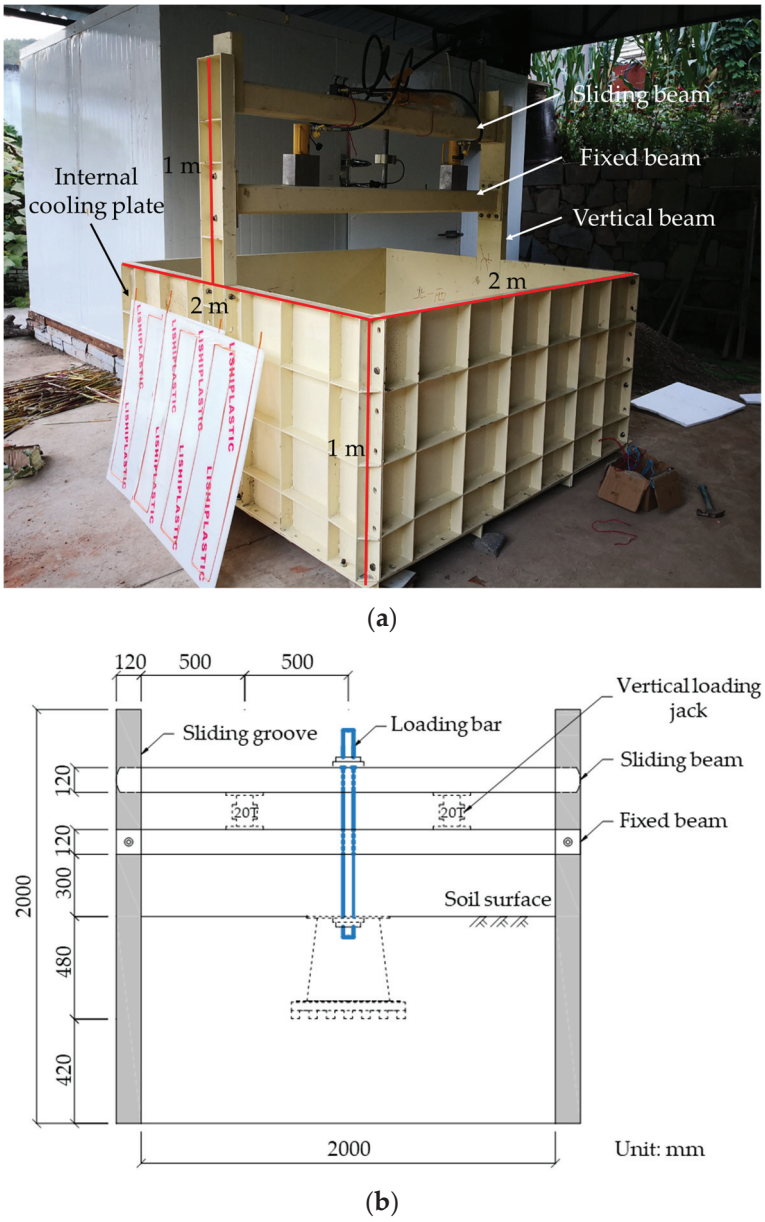

Figure 3. Test box and loading system: (**a**) photo of test box and (**b**) schematic drawing of loading system.

2.2.2. Refrigeration and Insulation Facilities

The refrigeration and insulation facilities consist of three parts:

(1) An external refrigerator (Figure 4a) with the refrigerating capacity of 18 kW and the lowest refrigeration temperature of −30 °C is used to reduce the ambient temperature of the chamber (Figure 4c).

(2) An internal cycle refrigerator (Figure 4b), whose corresponding parameters are 3.5 kW and −50 °C, serves for controlling the temperature of the box walls. This machine can cool and drive the coolant to circulate in 22 mm diameter U-shaped copper tubes, which are placed on the internal cooling plate (Figure 3a). A total of four plates are embedded on the vertical walls of the test box.

(3) The constant temperature chamber (Figure 4c) is composed of five rock-wool boards which are 10 cm thick. The length, width and height of the chamber are 4 m, 4 m, and 3 m, respectively.

(**a**) (**b**) (**c**)

Figure 4. Refrigeration system: photo of (**a**) external refrigerator, (**b**) internal cycle refrigerator, and (**c**) constant temperature chamber.

2.2.3. Monitoring Apparatuses

For all the tests, some data need to be monitored, including temperature, load, and displacement. A total of 18 temperature sensors, whose measuring range is from −50 °C to 200 °C and accuracy is 0.01 °C, are buried in the soil according to the arrangement of Figure 5. One S-shaped load cell with a range from 0 kN to 500 kN and an accuracy of 0.01 kN is selected to monitor the uplift load. Five electronic displacement sensors (numbered D1 ~ D5) with a range of 100 mm and sensitivity of 0.001 mm are arranged as illustrated in Figure 5. The average reading of two sensors (D1 and D2) is taken as the displacement of the foundation head. All the monitoring instruments had been calibrated before the test.

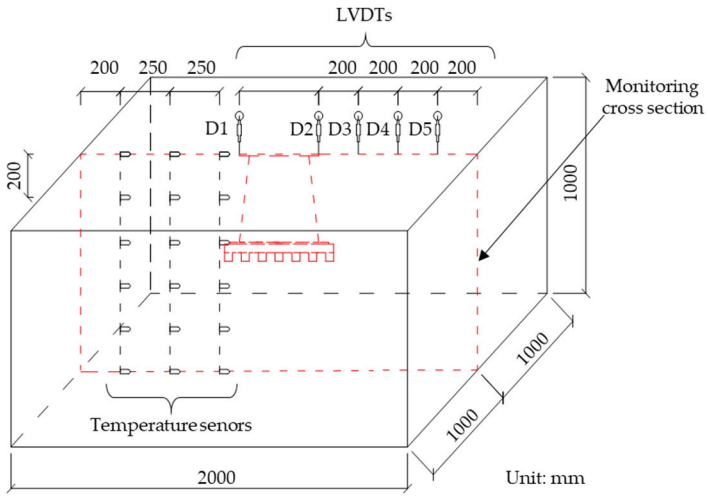

Figure 5. Location of monitoring cross section and the arrangement of electronic sensors.

2.3. Test Procedure: Freezing and Loading Process

The period of one test procedure is about 18 days, including two days for soil preparation and instrument installation, seven days for freezing, one day for loading, and ten days for soil thawing. In the first two days, the test soil needs to be prepared and then filled into the test box. The specific process is as follows:

(1) According to the data of Table 1 and the volume of the test box, about 6 kg test soil with moisture content of 10.4% are prepared and then sealed with plastic film for 24 hours, to make the moisture distribution uniform.

(2) Lay the soil into the test box layer by layer. Each layer is filled with 100 mm and then compacted to 80 mm to ensure the compactness is 80% and the distributions is uniform. When the buried thickness reaches 420 mm, the foundation will be placed in the center of the test box, and then the soil is filled again until it reaches 1000 mm. Overall, 18 temperature sensors are buried at this stage.

(3) Install the surface monitoring instruments and prepare for freezing.

In the next seven days, the soil will be frozen at a temperature of −5 °C, −10 °C, or −15 °C. These three temperatures are designed according to the ambient temperatures in Hailar (Figure 6). For example, the −10 °C, which is set to simulate the temperatures of this region in March and November. During the freezing process, the refrigeration temperature of the external refrigerator and the internal cycle refrigerator are all set to −10 °C, whereas the fluctuation values are 1 °C and 0.1 °C, respectively. The experience of the early commissioning test shows that the soil will be all frozen and the frost heave displacement will be stable after seven days of freezing.

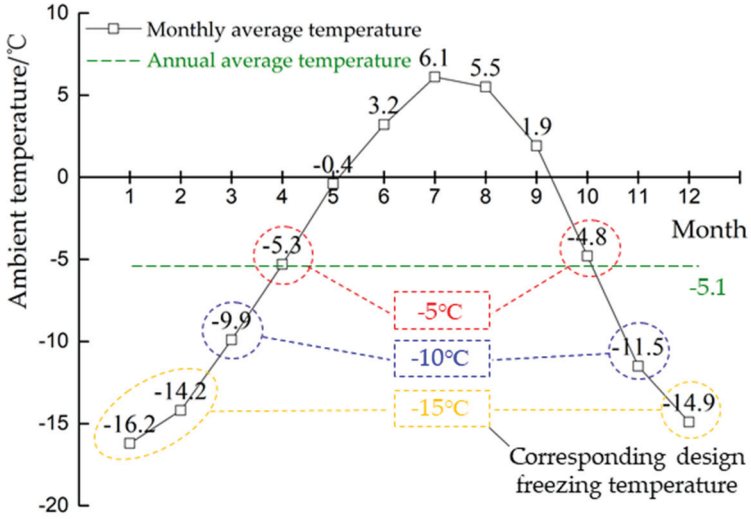

Figure 6. Ambient temperatures in Hailar, Inner Mongolia, China.

On the tenth day of the test cycle, the loading process is usually carried out. The slowly maintained loading method that is adopted by many researchers [27–30] is used in this work: first, the single-stage load increment is determined according to 10% of the predicted ultimate load; then, the static monotonic loading without cycle is carried out, and the displacement increment of the foundation after each load is recorded, until a certain displacement rate is reached. The time of each loading stage is maintained at 30 minutes, and then the next loading increment will be applied when the foundation displacement tends to be stable. In the last ten days (the number of days is greatly affected by the weather and the environment, but usually not more than ten days), the soil needs to be thawed, dispersed, and properly dried for the next test. The whole test lasted for about four months.

2.4. Test Results and Analysis

2.4.1. Results of Freezing Test: Temperature Field and Soil Frost Heave

Figure 7 illustrates the temperature distribution of frozen soil at −5 °C, −10 °C, and −15 °C. It is obvious that the temperature of the soil near the surface ground or the box walls is lower, but all the soil is completely frozen. Meanwhile, the distribution of the surface frost-heave displacements also shows the same law, as depicted in Figure 8. The soil temperature near the box wall is the lowest, and

the corresponding frost heave displacement is the largest, reaching 0.74 mm, 0.80 mm, and 2.01 mm, respectively. At the same time, the displacement at the top of the foundation is 0.36 mm, 0.40 mm, and 0.56 mm, respectively.

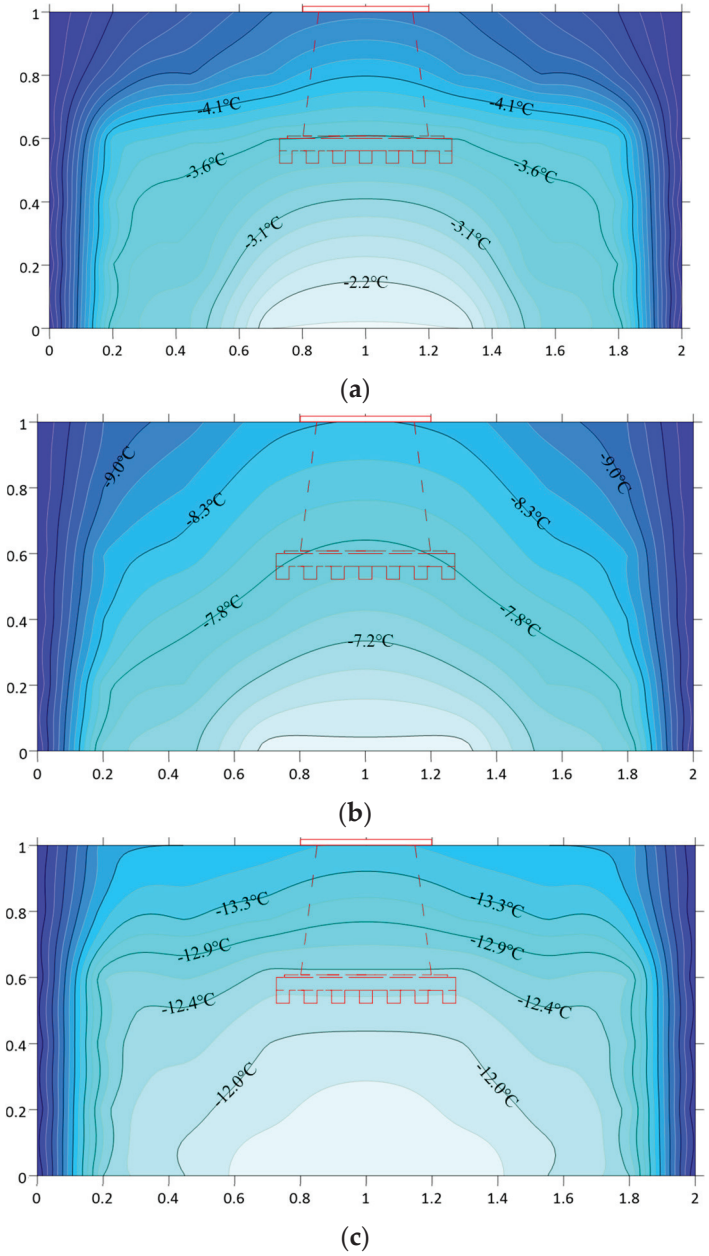

Figure 7. Temperature distribution of frozen soil at (**a**) −5 °C, (**b**) −10 °C, and (**c**) −15 °C.

It should be noted that there is no field soil temperature distribution as a comparison, but the temperature gradient distribution in Figure 7 is similar to the long-term observation results of Guo et al. [8] and Mu et al. [31] on the Qinghai Tibet Plateau, and it also conforms to the heat transfer law proposed by Li et al. [32] Therefore, it is considered that the freezing tests can simulate the temperature distribution similarly to the field.

2.4.2. Results of Loading Test: Uplift Load Versus Displacement Curves

Figure 9 shows the curves of uplift load versus displacement at three freezing temperatures. Based on the characteristics of these curves, the ultimate uplift load of the foundation can be determined by

many methods, including: (1) mathematical fitting analysis [33]; (2) image analysis [34]; and (3) limited displacement [35]. In this study, the L_1-L_2 method, a method of image analysis, which is selected in the relevant researches similar to the loading conditions [28–30]. This method divides the curve into three stages: the initial elastic stage (OA), the transition stage (AB), and the final failure stage (BC). The starting point B of the final failure stage is taken as the value point of the ultimate uplift load of the foundation, and the results are indicated in Figure 8: The load increases with the decrease of freezing temperatures, and the growth rate corresponding to the two decreases are 94.2% and 38.1%, respectively, but the corresponding displacement hardly increases. The main reason is that the elastic modulus of the soil increases with the decrease of temperature, which enhances the bearing capacity provided by the unit strain of soil. In addition, the bearing capacity is also affected by the size of the foundation. Therefore, the numerical modeling is carried out in Section 3.

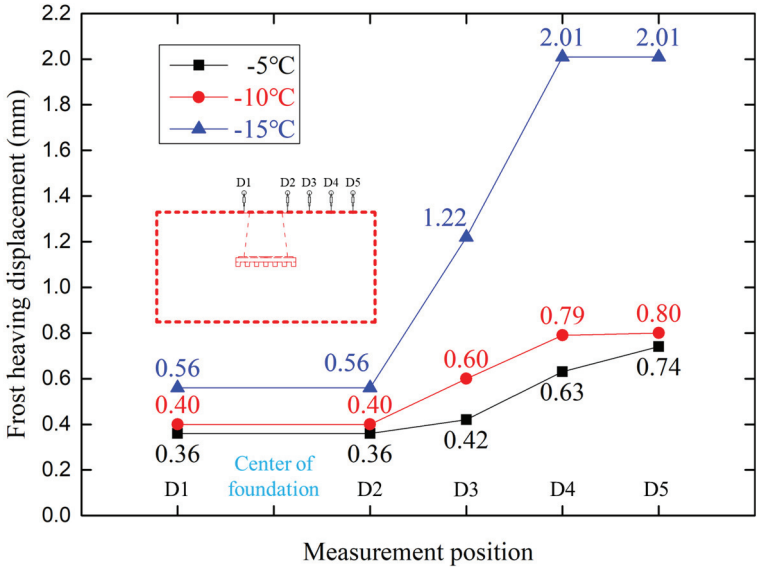

Figure 8. Frost heaving displacement of test pier and frozen soil surface.

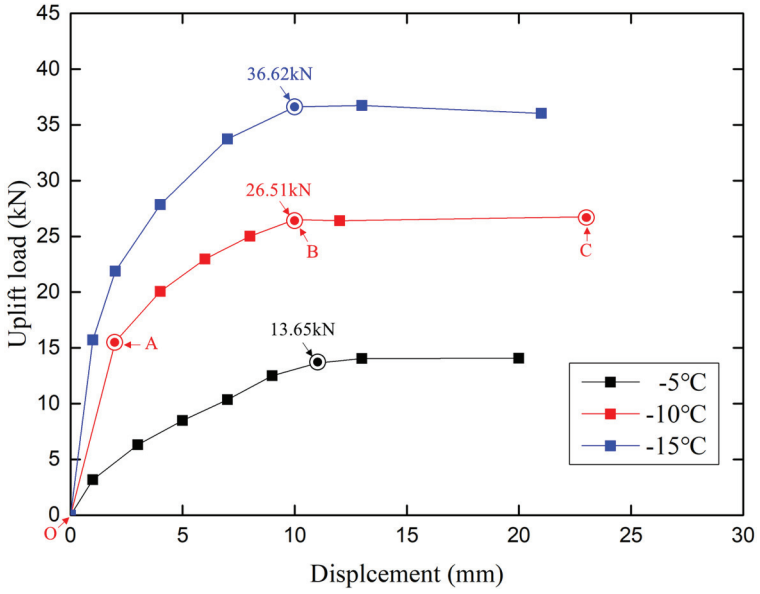

Figure 9. The uplift load versus displacement curves at three freezing temperatures.

3. Numerical Modeling

Numerical modeling is a common method for analyzing the bearing capacity of foundations [36–38], which has the advantages of an unlimited number of test samples and a high flexibility of the simulation scheme.

3.1. Modeling Scheme

The simplified diagram of the cone-cylinder foundation is illustrated in Figure 10. Firstly, a validation model is established according to the data of reduced-scale modeling test, to verify the feasibility and accuracy of simulation. Secondly, the simulation foundations of nine sizes are established based on the validation model, for studying the influence of three-dimensional factors, including the ratio of the depth to bottom width ($\lambda = h_t/D_t$), the top diameter of the cone-cylinder (d), and the bottom diameter of the cone-cylinder (D), on the bearing capacity of foundations. At the same time, the values and combinations of λ, d, and D refer to the orthogonal principle, as listed in Tables 4 and 5. The e and m for all foundations are 0.02 m and 0.01 m, respectively.

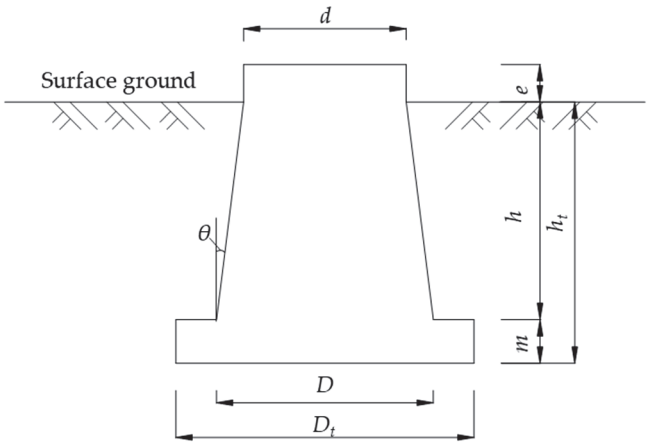

Figure 10. Dimensional sketch of cone-cylinder foundation.

Table 4. Levels of three dimension factors.

Levels	Factors		
	λ	d (m)	D (m)
1	1.0	0.2	0.4
2	2.0	0.3	0.5
3	3.0	0.4	0.6

Table 5. Dimensional combination of the foundations of nine sizes (V is the foundation volume).

No.	λ	d (m)	D (m)	h_t (m)	D_t (m)	θ (°)	V (m^3)
no.1	1.0	0.2	0.4	0.5	0.5	11.3	0.050
no.2	1.0	0.3	0.5	0.6	0.6	9.5	0.098
no.3	1.0	0.4	0.6	0.7	0.7	8.1	0.170
no.4	2.0	0.2	0.5	1.2	0.6	7.1	0.143
no.5	2.0	0.3	0.6	1.4	0.7	6.1	0.260
no.6	2.0	0.4	0.4	1.0	0.5	0.0	0.141
no.7	3.0	0.2	0.6	2.1	0.7	5.4	0.315
no.8	3.0	0.3	0.4	1.5	0.5	1.9	0.159
no.9	3.0	0.4	0.5	1.8	0.6	1.6	0.309

3.2. Geometric Modeling

All the grids are generated by the editor built in the FLAC 3D software. Figure 11a depicts the mesh of frozen soil, foundation, and the interface between them. The interface (red mesh in Figure 11a) is set as "hard", to prevent the tension forming. The detailed method is to set the stiffness to larger, which is set to 10 times of the elastic modulus of frozen soil according to the manual of FLAC 3D software. Figure 11b illustrates the boundary conditions: only the top surface is free; the displacement and velocity of the other five surfaces are all fixed alone the corresponding direction. Figure 12 illustrates the schematic diagram of nine simulation foundations. The number of zones and grid points (GPs for short) of the complete mesh containing frozen soil zones is indicated in Figures 11a and 12. It should be noted that the heat-generating sources are arranged on the top and surrounding surfaces of soil zones, whereas the bottom surface is free. This arrangement is the same as the indoor test.

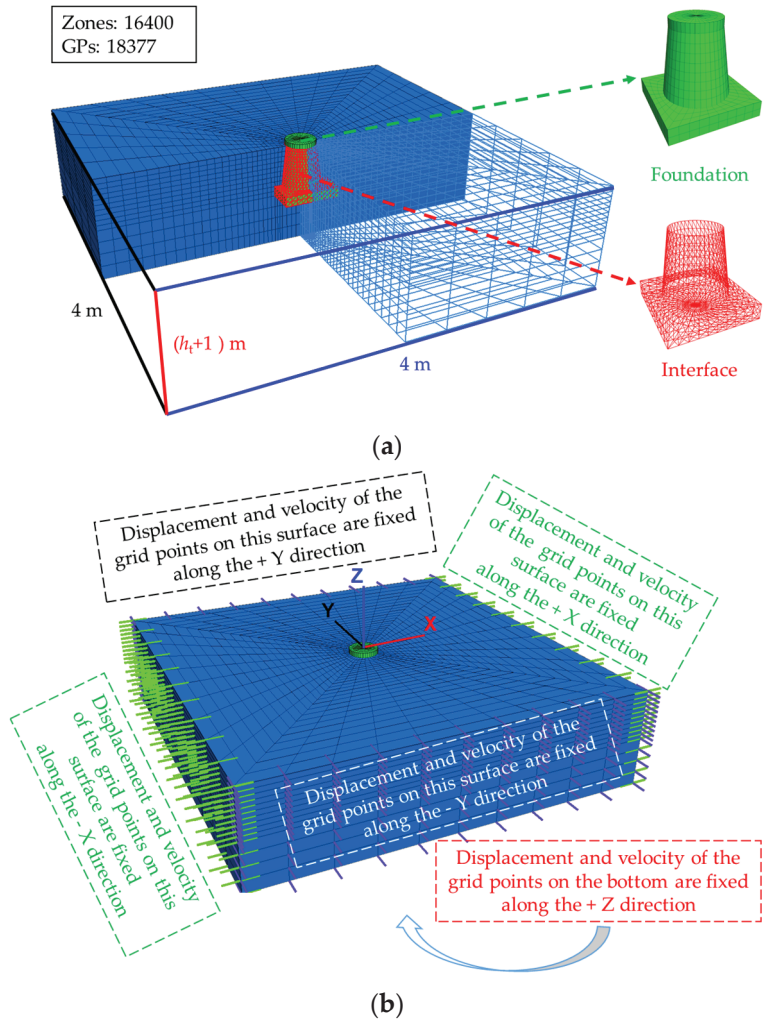

Figure 11. The diagram of mesh generation: (**a**) foundation, interface, and sizes and (**b**) boundary conditions.

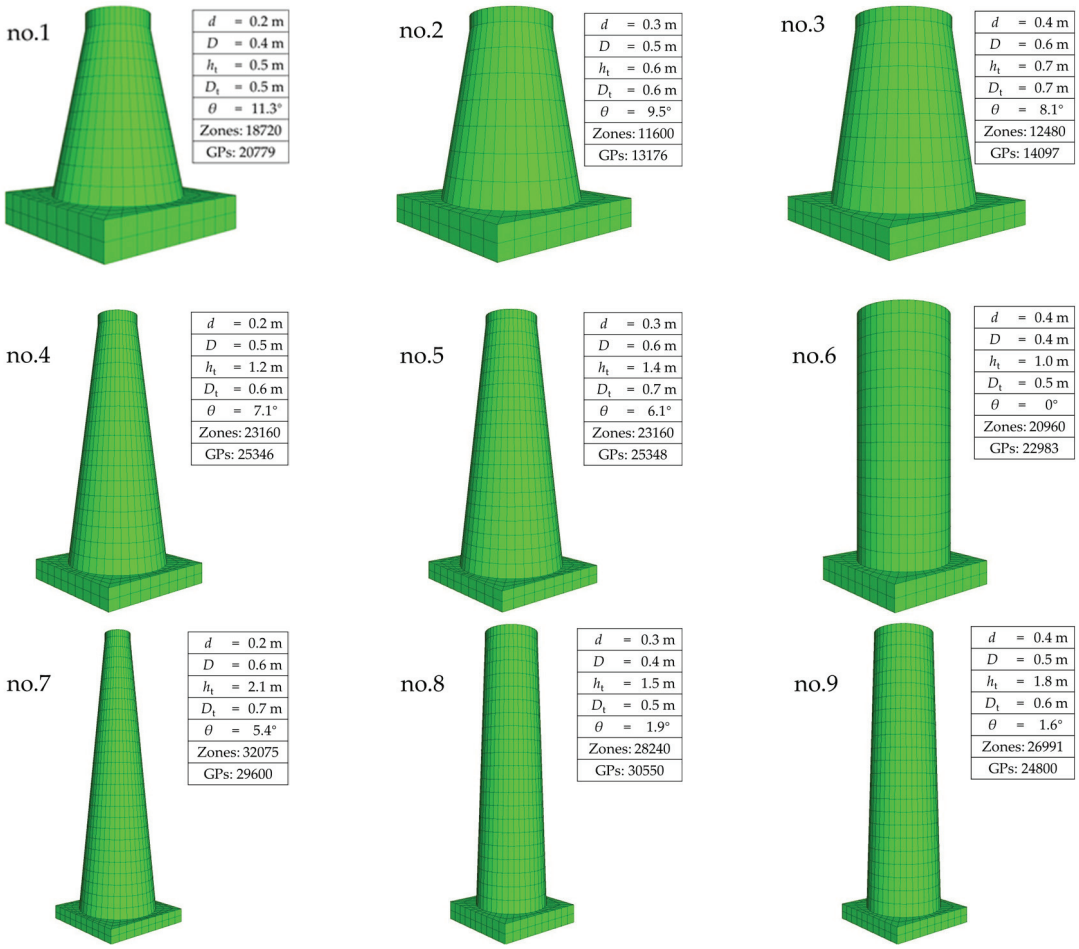

Figure 12. Schematic diagram of nine simulation foundations

3.3. Material Modeling

3.3.1. Physical and Mechanical Parameters

In this section, the material parameters of the frozen soil, the simulation foundation, and the interface between them are described. Frozen soil is approximately set as elastic-plastic material, and Mohr–Coulomb is selected as the failure criterion. The physical and mechanical parameters of frozen soil are measured according to the methods of ASTM D7300-18 [25] in the laboratory, including the uniaxial compression test and the direct shear test. The flow of uniaxial compression test of frozen soil is as follows: (1) nine soil samples with moisture content of 10.4% and compactness of 80% are prepared in nine test boxes with a diameter of 60 mm and a height of 125 mm; (2) after the sample is frozen at the corresponding freezing temperature (−5 °C, −10 °C, or −15 °C) for 48 h, it is installed on the MTS low-temperature testing machine and then kept at the same temperature for 24 h; (3) apply axial compressive load to the soil sample until it is damaged. Similarly, the direct shear tests are carried out on six soil samples after freezing for 48 h. The vertical pressures are set to 50 kPa, 100 kPa, 150 kPa, 200 kPa, 300 kPa, and 400 kPa, respectively, and the shear rate is 1 mm/min. The results are listed in Table 6.

Table 6. Physical and mechanical parameters of frozen soil at three temperatures.

Temperature (°C)	γ (kN/m^3)	E (MPa)	Poisson's Ratio	c (kPa)	φ (°)
−5	17.5	8.4 7.1 7.3	0.19 0.24 0.24	130.0 126.4	21.0 20.2
Mean value		7.6	0.22	128.2	20.6
−10	17.1	15.7 15.3 14.6	0.18 0.19 0.22	140.5 134.7	23.7 20.9
Mean value		15.2	0.20	137.6	22.3
−15	16.3	22.3 22.8 23.2	0.19 0.18 0.17	148.7 164.1	23.1 30.7
Mean value		22.8	0.18	156.4	26.9

The foundation is modeled as liner elastic material, whose elastic modulus is 210 GPa and the Poisson's ratio is 0.25. The density of solid simulation foundation needs to be converted to maintain the same weigh as the hollow test foundation (Figure 1), and the converted density is 688 kg/m^3. The parameters of the interface are determined according to the manual of FLAC 3D software: The normal and tangential stiffness are taken as 10 times of the soil's elastic modulus, whereas the c and φ are taken as 0.7 times of the corresponding values of the soil. The value results are listed in Table 7.

Table 7. Parameters of the interface at three temperatures.

MateRial	Temperature (°C)	Normal Stiffness (MPa/m)	Tangential Stiffness (MPa/m)	c (kPa)	φ (°)
Interface	-5	76	76	89.7	14.4
	-10	152	152	96.3	15.6
	-15	228	228	109.5	18.8

3.3.2. Thermodynamic Parameters

The temperature module of FLAC 3D software can simulate the transient heat conduction of materials, as well as the displacement and stress caused by the development of temperature. The module has the following characteristics: (1) any mechanical model can be used with the temperature model; (2) the change of temperature is controlled by the heat sources attached to or embedded in the zones; (3) the change of temperature can cause the change of zones stress, but on the contrary, the change of zones stress will not change the distribution of temperature; (4) the thermal conductivity and frost heave rate of soil are constant during freezing; and (5) the expansion effect of the frozen soil can be simulated by setting the heating power of the heat source and the expansion coefficient of the soil as negative values. In this simulation, the heating power of the heat source is set to 18 W/m.

The soil is fine-grained silt that is well graded (Table 1), so the thermal model to soil zones is set as isotropic heat conduction, i.e., the temperature decreases at the same rate in all directions. The thermal conductivity is 1.07 W/m·K, the frost heave rate is -5×10^{-5}, and the specific heat is 500 J/kg·K. The foundation is modeled as null thermal model, so that it will not produce displacement and stress with the decrease of temperature.

3.4. Validation for Simulation Model

According to the data of the reduced-scale modeling test, the feasibility and accuracy of the simulation are verified from two aspects: the frost heave displacements of soil and the load-displacement curves. The verification criteria refer to the method proposed by [39]: (1) the relative error of the frost

heave displacements; (2) the coincidence of load-displacement curves; and (3) the relative error of ultimate uplift loads. Figure 13 illustrates the comparison results of the frost heave displacements: the mean values of relative error at three temperatures are 3.7%, 9.2%, and 14.4%, respectively. Hence, the overall mean error is 9.1%. Figure 14 depicts the verification results of load-displacement curves: the minimum relative error of ultimate uplift load is 2.0%; the maximum is 12.9%; and the average is 5.9%. In conclusion, the results of the numerical simulation are basically consistent with those of the reduced-scale modeling tests.

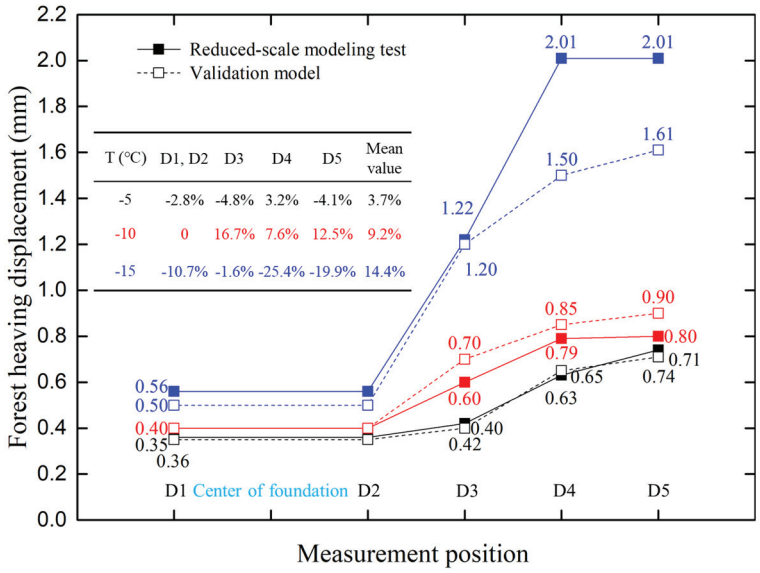

Figure 13. Comparison of frost heave displacement between numerical modeling and reduced-modeling tests.

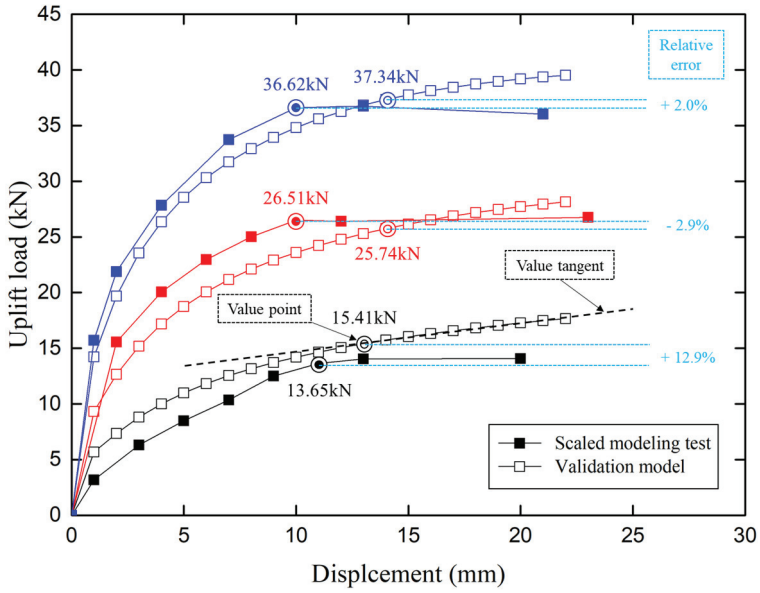

Figure 14. Verification results between the numerical modeling and the reduced-modeling tests.

3.5. Simulation Results and Analysis

3.5.1. Ultimate Uplift Load

The simulation of foundations of nine sizes are carried out based on the validation model. The ultimate uplift loads of nine foundations at three freezing temperatures are illustrated in Figure 15.

Obviously, with the decrease of freezing temperature, the ultimate bearing capacity of the foundation is improved, and the average growth rates corresponding to the two decreases are 64.8% and 50.7%, respectively. At the same time, the correlation coefficient between foundation bearing capacity and volume is calculated based on the following formula:

$$\rho_{TV} = \frac{Cov\,(T, V)}{\sqrt{D(T)}\sqrt{D(T)}} \tag{1}$$

where the T is the ultimate uplift load, V is the volume of foundation, Cov is the abbreviation of covariance, and D means the variance.

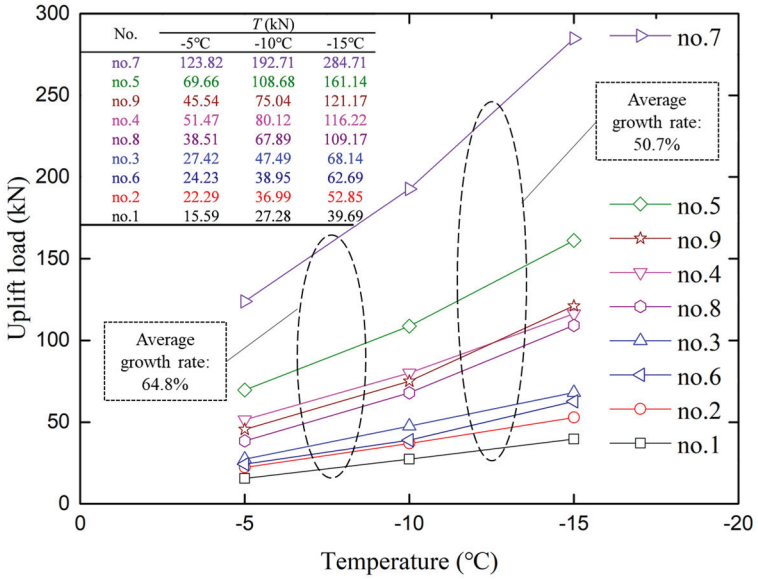

Figure 15. Ultimate uplift load of foundations of nine sizes at three freezing temperatures.

The calculation results of correlation coefficients at three temperatures are 0.77, 0.78, and 0.81, respectively, indicating that the bearing capacity of the foundation is positively related to the foundation volume. Hence, it is necessary to further compare the effect degree of the dimension factors (λ, d, and D). Taking the analysis of range for factor λ as an example, the calculation formulas are as follows:

$$\begin{cases} \mathrm{I}_{\lambda} = Average(15.59, 22.29, 27.42) = 21.77 \\ \mathrm{II}_{\lambda} = Average(51.47, 69.66, 24.23) = 48.45 \\ \mathrm{III}_{\lambda} = Average(123.82, 38.51, 45.54) = 69.29 \end{cases} \tag{2}$$

The value of R is calculated as follows:

$$R_{\lambda} = Max(\mathrm{I}_{\lambda}, \mathrm{II}_{\lambda}, \mathrm{III}_{\lambda}) - Min(\mathrm{I}_{\lambda}, \mathrm{II}_{\lambda}, \mathrm{III}_{\lambda}) = 69.29 - 21.77 = 47.52 \tag{3}$$

The values of R_d and R_D can be calculated in the same way. The results are indicated in Figure 16: at −5 °C, the R of λ and D are equal, which means that the influence degree of the two cannot be compared. Therefore, the analysis of variance is selected for further comparison. The calculation results are listed in Table 5; the influence degree of each factor can be compared by comparing the standard deviation. At −5 °C, the standard deviation of λ is smaller than that of D, indicating that the latter has greater influence on the bearing capacity than the former. At −10 °C and −15 °C, the influence order is λ, D, and d, which is consistent with the result of range analysis.

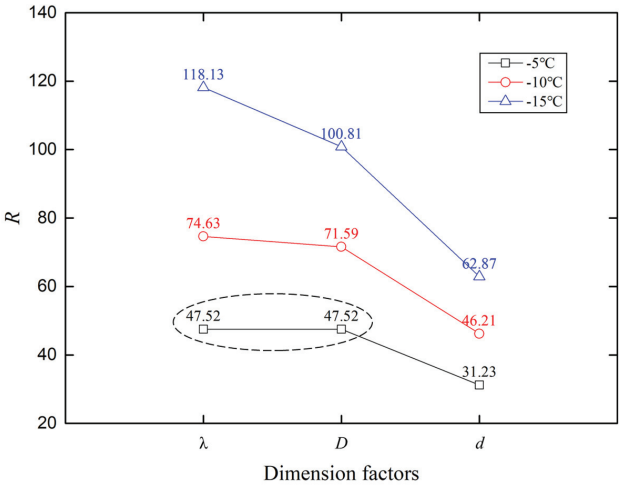

Figure 16. Calculation results of range analysis.

In order to further analyze whether the influence of dimension factors is significant, the joint hypothesis (F-test) is adopted. There are four cases of the comparison between the calculated F and critical F: (1) $F > F_{0.01}$, the influence of factors is particularly significant; (2) $F_{0.01} \geq F > F_{0.05}$, significant influence; (3) $F_{0.05} \geq F > F_{0.1}$, have a certain impact; and (4) $F_{0.1} \geq F$, unable to judge the degree of impact. As shown in Table 8, all the calculated values of F are less than the value of $F_{0.1}$ (2,2), indicating that all the dimension factors are not the significant factors.

Table 8. The results of variance analysis and F-test.

Temperature (°C)	Source of Variance	Standard Deviation	F-Test		
			Degree of Freedom	F Calculated Value	F Critical Value
−5	λ	1702.2	2	3.56	$F_{0.01}$ (2,2) = 99.0 $F_{0.05}$ (2,2) = 19.0 $F_{0.1}$(2,2) = 9.0
	d	752.1		1.49	
	D	1796.1		3.37	
−10	λ	4178.5	2	4.22	
	d	1634.8		1.65	
	D	4113.9		4.15	
−15	λ	10465.9	2	5.14	
	d	3024.1		1.49	
	D	8206.0		4.03	

3.5.2. Failure Mechanisms for Frozen Soil

Nazir et al. [40] tested the uplift bearing capacity of a series of enlarged base piers in both loose and dense sand packing, and analyzed the failure mechanisms of piers using a glass box, for observing the shape of the failure surface. Similarly, the failure mechanisms of frozen soil will be described by analyzing the plastic zones under ultimate bearing state. As depicted in Figure 17, three typical failure mechanisms are summarized, based on the comparison of the plastic zones of nine foundations at three temperatures:

(1) The T-mode with the T-shaped plastic zones is illustrated in Figure 17a. The shear failure occurs from the bottom to the top along the cone-cylinder surface, and forming a cylinder plastic region. Then, the lifting effect occurs on the upper soil and causing the tensile failure. Finally, the T-shaped plastic zones are formed.

(2) The V-mode is indicated in Figure 17b. The failure law of this mode is similar to that of the T-mode, except that the ratio of shear failure zones to tensile failure zones is reduced. The number of tensile failure zones is obviously increased.

(3) The U-mode is shown in Figure 17c. The plastic zones of this mode are larger than the former two modes. Most of the zones are tensile failure, while shear failure zones only account for a small part.

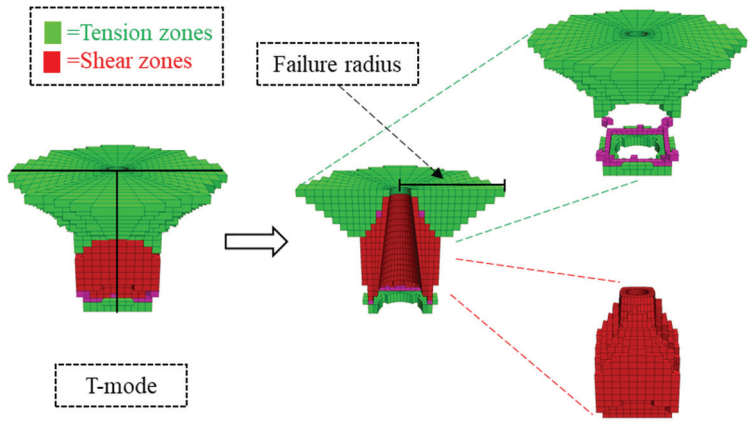

(**a**)

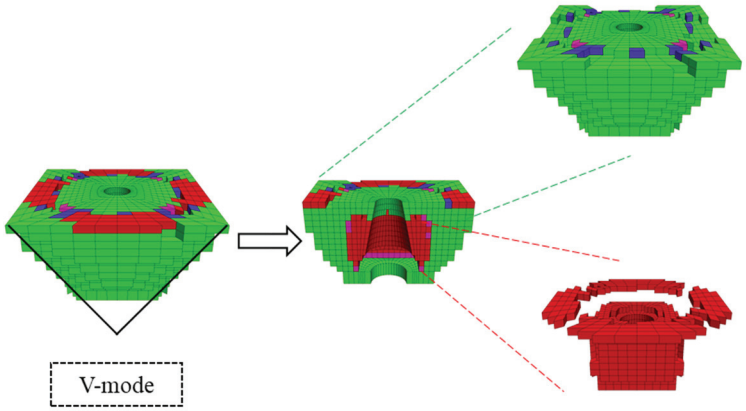

(**b**)

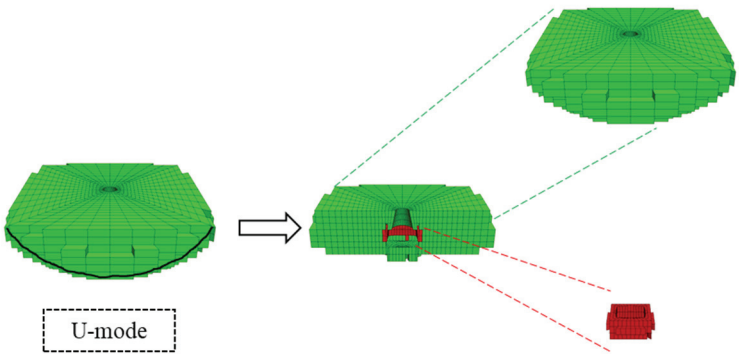

(**c**)

Figure 17. Three typical failure mechanisms of frozen soil: (**a**) T-mode; (**b**) V-mode; and (**c**) U-mode.

The distribution of these three modes is indicated in Figure 18: (1) at −5 °C, the failure mode of soil affected by dimension factors, especially λ. The failure mechanisms corresponding to $\lambda = 1$ and $\lambda > 1$ are V-mode and T-mode, respectively; (2) at −10 °C, the failure mechanisms of all foundations tend to

be the same, showing a transition mode between V-mode and U-mode; (3) at −15 °C, the U-mode is found in all nine foundations.

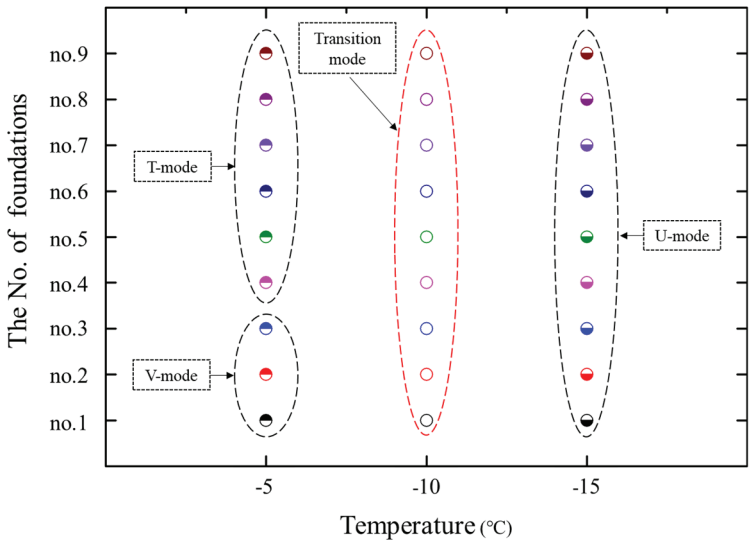

Figure 18. Distribution of T-mode, V-mode, and U-mode of nine foundations at three temperatures.

Meanwhile, the failure radii of 18 plastic zones are counted and illustrated in Figure 19: the radii are improved with the decrease of freezing temperature, and the average growth rates corresponding to the two decreases are 40.3% and 20.8%, respectively.

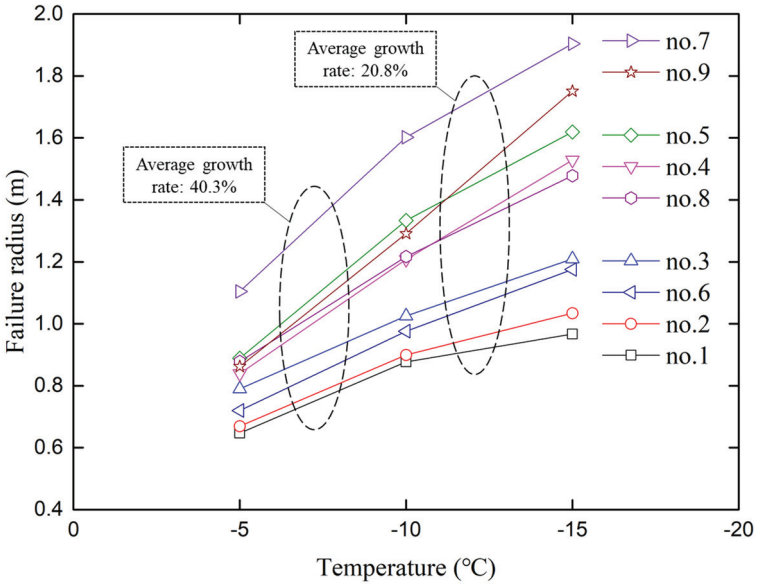

Figure 19. Change curve of failure radii of foundations of nine sizes at three temperatures.

In summary, the failure mechanisms of frozen soil are affected by the freezing temperatures and the foundation sizes at the same time, and the influence of the latter gradually weakens with the decrease of the former.

4. Comprehensive Analysis

In this section, the results of indoor tests and numerical simulations are synthetically analyzed. Theoretically, the ultimate bearing capacity of the foundation is determined by two aspects: the physical and mechanical properties of soil and the material strength of the foundation, and the former is usually

the main decisive factor. In this study, the latter, i.e., the foundation of steel, is treated as rigid body and exhibit the uplift failure mode proposed by [41]. Compared with ordinary soil, the frozen soil has three main effects: (1) the cementation between soil particles and ice crystals increases significantly, while the elastic modulus increases and the Poisson's ratio decreases; (2) the friction between the soil and foundation increases due to the change of soil parameters; and (3) the cohesive force of soil to foundation increases with the increase of the cementation between ice crystal and foundation surface. Both of the above effects will increase with the decrease of temperature, but will gradually stabilize with the decrease of unfrozen water in soil. Correspondingly, in the early stage of loading, the cementation force work first. With the loading, the friction force between soil and foundation gradually participates in the bearing, and then transfers the load to the soil particles. At this time, the strength of the soil begins to play a role in the loading process and cracks appear. The above-mentioned bearing sequence can be used to explain the three failure mechanisms. For the T-mode, the cylinder shear plastic region indicates that the force of cementation and friction, especially the latter, bear a large proportion in the load bearing. For the V-mode and U-mode, this proportion will gradually decrease.

In addition, we think that the alteration of foundation sizes will not change the bearing sequence, but instead change the magnitude and duration of the force of cementation and friction. Whereas when the mechanical strength of frozen soil increases to a certain extent with the decrease of temperature, the soil will bear most of the uplift load, while the effect of the force of cementation and friction is negligible. The corresponding test phenomenon is that all the foundations of nine sizes show the U-mode failure.

5. Conclusions

Given the influence of the dimension factors and freezing temperatures on the uplift bearing capacity of cone-cylinder foundation, this work carries out a series of reduced-scale modeling tests indoor and numerical simulations. The following conclusions can be drawn:

(1) Firstly, the uplift bearing capacity of the cone-cylinder foundation increases with the decrease of temperature, but this trend will slow down with the decrease of unfrozen water in soil. The influence of temperature is mainly reflected in three aspects: the cementation force between the ice crystal and the foundation surface; the friction between the soil and foundation surface; and the mechanical strength of soil. These three factors will participate in the bearing process one by one and ultimately work together.

(2) Secondly, the uplift bearing capacity of the cone-cylinder foundation is positively correlated with the dimension factors, and the correlation ranks as follows: the ratio of depth to bottom width ($\lambda = h_t/D_t$), the bottom diameter of the cone-cylinder (D), and the top diameter of the cone-cylinder (d), but none of the above three factors are significant, according to the results of the F-test.

(3) Additionally, the frozen soil failure mechanisms of cone-cylinder foundation can be divided into three categories: T-mode, V-mode, and U-mode. There are two rules in the evolution of these three modes. One is that the bearing proportion of the force of cementation and friction decreases gradually, while the phenomenon is that the range of shear zones decreases whereas that of tension zones increases. The other is that the bearing proportion of the soil strength increases gradually, while the failure range of frozen soil increases significantly. Furthermore, the distribution of these three modes is affected by the temperatures and dimension factors at the same time, and the influence of the latter gradually weakens with the decrease of the former.

(4) Lastly, in future work, more factors will be considered, including more freezing temperatures, more loading directions, and more dimensions of foundations. At the same time, the method of the indoor model test will be improved: the tangential frost heave will be measured, and the failure sliding profile of the frozen soil will be observed.

Author Contributions: Conceptualization, Y.H.; methodology, Y.H. and J.C.; formal analysis, Y.H. and J.C.; software, Y.H. and Q.D.; resources, Y.H. and Q.C.; data curation, Y.H.; writing—original draft preparation, Y.H.; writing—review and editing, Y.H., J.C. and W.S.; supervision, J.C.; validation, Y.H.; funding acquisition, Q.C. All authors have read and agreed to the published version of the manuscript.

Funding: This research was funded by the State Grid Corporation of China, under the project of Key Technologies of Assembled Module for Converter Station and Transmission Line Foundation in Frozen soil regions (GCB 17201700134).

Acknowledgments: We would like to thank Deng Ming of Tsinghua University for his sagacious advice in the theoretical analysis part. At the same time, I would like to thank Yang Xiaorui. She lets me believe that someone who is iridescent really exists in this world, and when you are met with great luck, nothing will ever compare.

Conflicts of Interest: The authors declare no conflict of interest.

References

1. Wei, M.; Guodong, C.; Qingbai, W. Construction on permafrost foundations: Lessons learned from the Qinghai–Tibet railroad. *Cold Reg. Sci. Technol.* **2009**, *59*, 3–11. [CrossRef]
2. Wu, Q.; Niu, F. Permafrost changes and engineering stability in Qinghai-Xizang Plateau. *Chin. Sci. Bull.* **2013**, *58*, 1079–1094. [CrossRef]
3. Wei, X.; Huang, C.; Wei, N.; Zhao, H.; He, Y.; Wu, X. The impact of freeze–thaw cycles and soil moisture content at freezing on runoff and soil loss. *Land Degrad. Dev.* **2019**, *30*, 515–523. [CrossRef]
4. Li, P.; Yu, Q.H.; Yan, F.Z.; Huang, Y.S.; Cheng, D.X. Main Problems and Solutions on Design and Construction of Qinghai-Tibet DC Transmission Project in Permafrost Region. In *Advances in Civil and Industrial Engineering, Pts 1–4*; Tian, L., Hou, H., Eds.; Trans Tech Publications Ltd.: Bäch SZ, Switzerland, 2013; Volume 353–356, pp. 515–523.
5. Zhang, J.; Ruan, G.; Su, K.; Zhang, H. Estimation on settlement of precast tower footings along the Qinghai-Tibet Power Transmission Line in warm permafrost regions. *Cold Reg. Sci. Technol.* **2016**, *121*, 275–281. [CrossRef]
6. Li, G.; Yu, Q.; Ma, W.; Chen, Z.; Mu, Y.; Guo, L.; Wang, F. Freeze-thaw properties and long-term thermal stability of the unprotected tower foundation soils in permafrost regions along the Qinghai-Tibet Power Transmission Line. *Cold Reg. Sci. Technol.* **2016**, *121*, 258–274. [CrossRef]
7. Yu, Q.; Zhang, Z.; Wang, G.; Guo, L.; Wang, X.; Wang, P.; Bao, Z. Analysis of tower foundation stability along the Qinghai–Tibet Power Transmission Line and impact of the route on the permafrost. *Cold Reg. Sci. Technol.* **2016**, *121*, 205–213. [CrossRef]
8. Guo, L.; Xie, Y.; Yu, Q.; You, Y.; Wang, X.; Li, X. Displacements of tower foundations in permafrost regions along the Qinghai–Tibet Power Transmission Line. *Cold Reg. Sci. Technol.* **2016**, *121*, 187–195. [CrossRef]
9. Wen, Z.; Yu, Q.; Zhang, M.; Xue, K.; Chen, L.; Li, D. Stress and deformation characteristics of transmission tower foundations in permafrost regions along the Qinghai-Tibet Power Transmission Line. *Cold Reg. Sci. Technol.* **2016**, *121*, 214–225. [CrossRef]
10. Gu, Q.; Yang, Z.; Peng, Y. Parameters affecting laterally loaded piles in frozen soils by an efficient sensitivity analysis method. *Cold Reg. Sci. Technol.* **2016**, *121*, 42–51. [CrossRef]
11. Qi, J.; Vermeer, P.A.; Cheng, G. A review of the influence of freeze-thaw cycles on soil geotechnical properties. *Permafr. Periglac. Process.* **2006**, *17*, 245–252. [CrossRef]
12. Lu, J.-F.; Yin, J.; Shuai, J. A model for predicting the frost-heave effect of a pile embedded in the frozen soil. *Cold Reg. Sci. Technol.* **2018**, *146*, 214–222. [CrossRef]
13. Wang, T.; Liu, J.; Tian, Y.; Lv, P. Frost jacking characteristics of screw piles by model testing. *Cold Reg. Sci. Technol.* **2017**, *138*, 98–107. [CrossRef]
14. Liu, J.; Lv, P.; Cui, Y.; Liu, J. Experimental study on direct shear behavior of frozen soil-concrete interface. *Cold Reg. Sci. Technol.* **2014**, *104*, 1–6. [CrossRef]
15. Wen, Z.; Yu, Q.; Ma, W.; Dong, S.; Wang, D.; Niu, F.; Zhang, M. Experimental investigation on the effect of fiberglass reinforced plastic cover on adfreeze bond strength. *Cold Reg. Sci. Technol.* **2016**, *131*, 108–115. [CrossRef]
16. Fei, W.; Yang, Z.J.; Sun, T. Ground freezing impact on laterally loaded pile foundations considering strain rate effect. *Cold Reg. Sci. Technol.* **2019**, *157*, 53–63.

17. Yang, Z.J.; Li, Q.; Horazdovsky, J.; Hulsey, J.L.; Marx, E.E. Performance and Design of Laterally Loaded Piles in Frozen Ground. *J. Geotech. Geoenviron. Eng.* **2017**, *143*, 06016031. [CrossRef]
18. Kulhawy, F.H.; Trautmann, C.H.; Beech, J.F.; O'Rourke, T.D.; McGuire, W. *Transmission Line Structure Foundation for Uplift-Compression Loading*; Rep. No. EPRI-EL-2870; Electric Power Research Institute: Palo Alto, CA, USA, 1983.
19. Reddy, K.M.; Ayothiraman, R. Experimental Studies on Behavior of Single Pile under Combined Uplift and Lateral Loading. *J. Geotech. Geoenviron. Eng.* **2015**, *141*, 04015030. [CrossRef]
20. Huang, G.; Yan, B.; Wen, N.; Wu, C.; Li, Q. Study on jump height of transmission lines after ice-shedding by reduced-scale modeling test. *Cold Reg. Sci. Technol.* **2019**, *165*, 102781. [CrossRef]
21. ASTM. *Standard Test Method for Direct Shear Test of Soils under Consolidated Drained Conditions*; ASTM D3080/D3080M-11; ASTM: West Conshohocken, PA, USA, 2011b.
22. ASTM. *Standard Test Methods for Specific Gravity of Soil Solids by Water Pycnometer*; ASTM D854-14; ASTM: West Conshohocken, PA, USA, 2014.
23. ASTM. *Standard Test Method for Laboratory Determination of Creep Properties of Frozen Soil Samples by Uniaxial Compression*; D5520-18; ASTM: West Conshohocken, PA, USA, 2018.
24. ASTM. *Standard Terminology Relating to Frozen Soil and Rock*; ASTM D7099-04; ASTM: West Conshohocken, PA, USA, 2018.
25. ASTM. *Standard Test Method for Laboratory Determination of Strength Properties of Frozen Soil at a Constant Rate of Strain*; ASTM D7300-18; ASTM: West Conshohocken, PA, USA, 2018.
26. ASTM. *Standard Test Methods for Laboratory Determination of Water (Moisture) Content of Soil and Rock by Mass*; ASTM D2216-19; ASTM: West Conshohocken, PA, USA, 2019.
27. Harris, D.E.; Madabhushi, G.S. Uplift capacity of an under-reamed pile foundation. *Proc. Inst. Civ. Eng. Geotech. Eng.* **2015**, *168*, 526–538. [CrossRef]
28. Lu, X.L.; Qian, Z.Z.; Yang, W.Z. Axial Uplift Behavior of Belled Piers in Sloping Ground. *Geotech. Test. J.* **2017**, *40*, 20150202. [CrossRef]
29. Lu, X.-L.; Qian, Z.-Z.; Zheng, W.-F.; Yang, W.-Z.Y. Characterization and uncertainty of uplift load-displacement behaviour of belled piers. *Geomech. Eng.* **2016**, *11*, 211–234. [CrossRef]
30. Qian, Z.-Z.; Lu, X.-L.; Yang, W.-Z.; Engineering, G. Comparative Field Tests on Straight-Sided and Belled Piers on Sloping Ground under Combined Uplift and Lateral Loads. *J. Geotech. Geoenviron. Eng.* **2019**, *145*, 04018099. [CrossRef]
31. Mu, Y.; Li, G.; Yu, Q.; Ma, W.; Wang, D.; Wang, F. Numerical study of long-term cooling effects of thermosyphons around tower footings in permafrost regions along the Qinghai-Tibet Power Transmission Line. *Cold Reg. Sci. Technol.* **2016**, *121*, 237–249. [CrossRef]
32. Li, G.Y.; Yu, Q.H.; Ma, W.; Mu, Y.H.; Li, X.B.; Chen, Z.Y. Laboratory testing on heat transfer of frozen soil blocks used as backfills of pile foundation in permafrost along Qinghai-Tibet electrical transmission line. *Arab. J. Geosci.* **2015**, *8*, 2527–2535. [CrossRef]
33. Chin, F.K. Estimation of the ultimate load of piles not carried to failure. In *Proc. 2nd Southeast Asian Conf. on Soil Engineering*; Southeast Asian Society of Soil Engineering: Singapore, 1970; Volume 81–92.
34. O'rourke, T.D.; Kulhawy, F.H. Observations on load tests for drilled shafts. In *Drilled Piers and Caissons II*; ASCE: Reston, VA, USA, 1985; pp. 113–128.
35. Fuller, F.M.; Hoy, H.E. Pile load tests including quick load test method, conventional methods, and interpretations. In *Vol. 333 of Proc. 49th Annual Meeting of the Highway Research Board*; Highway Research Board: Washington, DC, USA, 1970; pp. 74–86.
36. Lian, J.; Jiang, Q.; Dong, X.; Zhao, Y.; Zhao, H. Dynamic Impedance of the Wide-Shallow Bucket Foundation for Offshore Wind Turbine Using Coupled Finite-Infinite Element Method. *Energies* **2019**, *12*, 4370. [CrossRef]
37. Zhang, P.; Li, Y.E.; Lv, Y.; Ding, H.; Le, C. Bearing Capacity Characteristics of Composite Bucket Foundation Under Torque Loading. *Energies* **2019**, *12*, 2487. [CrossRef]
38. Zhou, L.; Ding, S.; Song, M.; Gao, J.; Shi, W. A Simulation of Non-Simultaneous Ice Crushing Force for Wind Turbine Towers with Large Slopes. *Energies* **2019**, *12*, 2608. [CrossRef]
39. Zekavati, A.-A.; Khodaverdian, A.; Jafari, M.-A.; Hosseini, A. Investigating performance of micropiled raft in foundation of power transmission line towers in cohesive soil: Experimental and numerical study. *Can. Geotech. J.* **2018**, *55*, 312–328. [CrossRef]

40. Nazir, R.; Moayedi, H.; Pratikso, A.; Mosallanezhad, M. The uplift load capacity of an enlarged base pier embedded in dry sand. *Arab. J. Geosci.* **2015**, *8*, 7285–7296. [CrossRef]
41. Pacheco, M.P.; Danziger, F.A.B.; Pinto, C.P. Design of shallow foundations under tensile loading for transmission line towers: An overview. *Eng. Geol.* **2008**, *101*, 226–235. [CrossRef]